I&EC research
Industrial & Engineering Chemistry Research

pubs.acs.org/IECR

Article

Ion-Exchange Resin-Templated Carbon Capture Sorbents with Hierarchical Pores

Ching-En Ku, Lu Liu, and Chen Zhang*

Cite This: https://doi.org/10.1021/acs.iecr.4c00479

Read Online

ACCESS | Metrics & More | Article Recommendations | Supporting Information

ABSTRACT: The pore structure of mesoporous silica is crucial to its application as a substrate for CO_2 capture sorbents. In this work, the synthesis of resin-templated silica, a new class of hierarchically meso-/macroporous silica for fabrication of CO_2 capture sorbents, was reported. Unlike the conventional acid-catalyzed synthesis of mesoporous silica using self-assembled surfactant or block copolymer templates, the resin-templated silica is derived from porous ion-exchange resin templates using a catalyst-free method that involves three simple steps of silane soaking, moisture exposure, and air calcination. The resin-templated silica reproduced the spherical shape of the porous ion-exchange resin template. It was also found that pores in resin templates were crucial to creating mesoporosity in resin-templated silica. The resin-templated silica has simultaneous attractive surface area and pore volume, which were both substantially higher than those of the ion-exchange resin template. Impregnation of the mesopores and macropores by polymeric amine provided novel amine-oxide sorbents for CO_2 capture, that is, resin-templated sorbents. The resin-templated sorbents impregnated using a 15 wt % polyethylenimine (PEI)/methanol solution showed competitive direct air capture (at 400 ppm) performance with a CO_2 sorption capacity of 2.1 mmol of CO_2/g of SiO_2 and amine efficiency of 0.11 mol of CO_2/mol of N at an amine loading of 0.83 g of PEI/g of SiO_2.

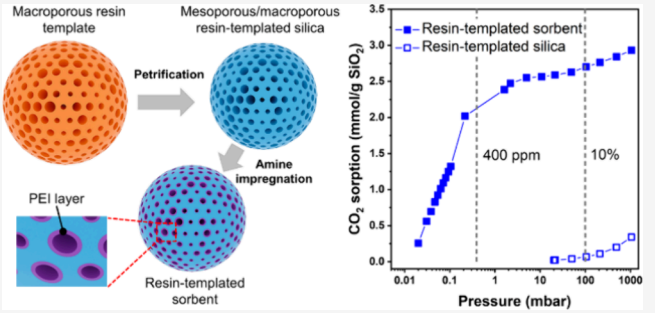

1. INTRODUCTION

Global surface temperature has increased by 0.8 °C since the 1970s and is predicted to increase by up to 4.8 °C by the end of the 21st century.[1] The temperature increase is largely attributed to rapidly rising CO_2 concentration in the atmosphere as a result of emission from fossil fuel combustion. The National Academies of Sciences, Engineering, and Medicine recommended prioritizing the advancement of direct air capture (DAC),[2] which is among the negative emission technologies (NETs) intended to slow global temperature rise. Direct air capture can rely on liquid solvents, solid sorbents, or electrochemical approaches.[3] Notably, the strong amine-CO_2 reaction provided by amine-oxide sorbents can allow selective CO_2 capture from ultradilute (~420 ppm of CO_2) ambient air.[4,5]

Amine-oxide sorbents are formed by introducing amines to mesoporous oxide (e.g., silica) substrates.[6,7] The strong acid−base reactions between CO_2 (a Lewis acid) and amines allow selective CO_2 sorption from other air components even at ultralow concentrations. Amine-oxide sorbents are classified based on the nature of amine-oxide interactions.[5] In class 1 sorbents, polymeric amines (e.g., polyethylenimines, PEI) are physically impregnated into the pores of oxide substrates.[8−12] Class 2 sorbents are typically formed via covalent bonds between the oxide surface hydroxyl groups and low-molecular-weight aminosilanes (e.g., 3-aminopropyltrimethoxysilane).[13] Class 3 sorbents mainly rely on in situ polymerization of amine monomers (e.g., aziridine) inside porous oxide substrates to form hyperbranched amino-oxides.[14] High CO_2 sorption capacity, fast sorption kinetics, and outstanding stability under sorption/desorption cycles are desired for amine-oxide sorbents for direct air capture. It has been shown that the direct air capture performance of amine-oxide sorbents is determined by a number of factors, including the pore structure and chemistry of oxide substrates, the nature of amine-oxide interactions, amine chemistry, operation conditions, and so forth.[4,15] Class 1 sorbents have so far been the most extensively studied due to easy fabrication and high CO_2 sorption capacity. However, class 1 sorbents are subject to amine leaching[4] and generally less stable than class 2 and 3 sorbents. Amine-oxide sorbents are highly versatile and compatible with diverse sorbent geometries. For example, in addition to being used in traditional packed beds, amine-oxide

Received: February 4, 2024
Revised: May 30, 2024
Accepted: June 11, 2024

sorbent particles can be dispersed in porous polymer hollow fiber matrix to provide structured hollow fiber sorbents.[16−19]

Mesoporous silica is popularly used as a substrate of amine-oxide sorbents. The pore size, surface area, and pore volume of the mesoporous silica substrate are important to the adsorption capacity and adsorption kinetics of amine-oxide sorbents. Mesoporous silica is traditionally synthesized by soft-templating[20] or hard-templating[21] methods, both relying on cationic surfactants or block copolymers. For example, ordered mesoporous silica (e.g., MCM-41 and SBA-15) with uniform mesopores (2 nm < d < 50 nm) is synthesized by the soft-templating method using self-assembly of silica species and micelles of cationic surfactants or block copolymers.[6,7,22−24] Following synthesis, the organic micelles can be removed by air calcination,[22] supercritical CO_2 extraction,[25] or washing[24] to provide uniform and tunable mesopores. In addition to ordered mesoporous silica, hierarchically meso-/macroporous silica and other oxides[26−32] have been used as substrates to fabricate amine-oxide sorbents for CO_2 capture. The macropores (d > 50 nm) can provide extra space for amine impregnation and sometimes improved sorption kinetics. For example, Kwon and co-workers[30] reported fabrication of hierarchically meso-/macroporous silica using a dual template method consisting of a combination of soft template (block copolymer) and hard template (spherical polystyrene bead). Amine impregnation of the dual-templated silica gave sorbents with a highly attractive CO_2 sorption capacity. Our recent work[33] showed that petrification of macroporous hollow fiber templates can give hierarchically micro-/meso-/macroporous silica hollow fiber membranes with both high surface area and large pore volume. The petrification process requires no catalyst and occurs by three simple steps: silane soaking, moisture exposure, and air calcination. It would be attractive to adapt the petrification method to fabricate hierarchically porous silica by using a broader range of polymer templates for a wider spectrum of separation applications.

Ion-exchange resins consist of cross-linked styrene-divinylbenzene or acrylic matrix functionalized by active sites.[34−36] By tuning the active site chemistry, cation-exchange resin (e.g., with sulfonic acid active sites) or anion-exchange resin (e.g., with tertiary amine active sites) can be made. Ion-exchange resins can be either nonporous (i.e., gel-type resin) or porous. The pores in porous ion-exchange resins provide rapid fluid transport for fast ion exchange or chemical reactions.[37,38] The pores also allow for petrification of the ion-exchange resin by providing space for silica formation. Here, we show that the petrification method can be adapted to fabricate hierarchically meso-/macroporous resin-templated silica using a porous ion-exchange resin as template. Unlike the aforementioned soft-templating or hard-templating methods, no surfactants or block copolymers are used. Amine impregnation of these novel resin-templated silica provided resin-templated sorbents potentially suitable for both direct air CO_2 capture and flue gas CO_2 capture.

2. MATERIALS AND METHODS

2.1. Materials. AmberLyst 15 cation-exchange resin (porous, hydrogen form), AmberLite FPC23H (porous, hydrogen form), and AmberLite IRC120 cation-exchange resin (gel-type, hydrogen form) were obtained from Sigma-Aldrich and dried under vacuum at 110 °C for 12 h before use. Polyethylenimine (branched, average molecular weight 800) was obtained from Sigma-Aldrich. Vinyltrimethoxysilane (VTMS, 97%, Gelest), methanol (anhydrous, Sigma-Aldrich), and hexane (anhydrous, mixture of isomers, Sigma-Aldrich) were used as received.

2.2. Synthesis of Resin-Templated Silica. Resin-templated silica was synthesized by the petrification of porous ion-exchange resin templates, which involves silane soaking, exposure to moisture, and air calcination. More specifically, the dried ion-exchange resin beads were soaked in a 10 wt % VTMS/hexane solution for 24 h. After the solution was decanted, the resin beads were allowed to dry in a fume hood for 12 h before being exposed to water vapor saturated air for another 24 h to provide treated ion-exchange resin. Resin-templated silica was obtained by calcining the treated ion-exchange resin in a Lindberg/Blue Moldatherm box furnace (Thermo Scientific, Waltham, MA) under continuous air flow (0.5 L/min) using the following heating protocol: (1) room temperature to 600 °C (5 °C/min); (2) dwelling at 600 °C for 120 min; (3) naturally cool down to room temperature.

2.3. Characterizations. Scanning electron microscopy (SEM) and energy-dispersive X-ray (EDX) analyses were performed using a Tescan GAIA3 FEG scanning electron microscope. Particle size distribution curves were obtained by analyzing the SEM images using ImageJ. Nitrogen physisorption (77 K) was performed with an ASAP 2020Plus physisorption analyzer (Micromeritics, Norcross, GA). Ion-exchange resin samples were degassed at 120 °C for 12 h prior to isotherm collection. Resin-templated silica samples were degassed at 200 °C for 12 h prior to isotherm collection. A nonlocal density functional theory (NLDFT) model (N_2 [77 K], cylindrical pore, oxide surface) was used to calculate the pore size distribution curves using the nitrogen physisorption isotherms. Water vapor sorption measurements were carried out in a VTI-SA+ vapor sorption analyzer (TA Instruments, New Castle, DE). Fourier transform infrared spectra were obtained by using a ThermoNicolet Nexus 670 FT-IR spectrometer. Powder X-ray diffraction patterns were recorded using a Bruker D8 Advance Lynx powder diffractometer (LynxEye PSD detector, sealed tube, Cu Kα radiation with a Ni β-filter). Thermogravimetric analysis (TGA) was performed by using a Shimadzu TGA50 thermogravimetric analyzer. Mercury intrusion porosimetry was performed by the Particle Testing Authority (Micromeritics, Norcross, GA) using an AutoPore V9600 mercury intrusion porosimetry analyzer.

2.4. Fabrication of Resin-Templated Sorbents. Resin-templated sorbents were formed by polyethylenimine (PEI) impregnation of resin-templated silica. Resin-templated silica was first dried in a vacuum oven for 12 h to remove adsorbed moisture. The PEI impregnation was carried out by soaking the dried resin-templated silica in PEI/methanol solutions for 24 h. After the solution was decanted, the PEI-impregnated resin-templated sorbent was dried in a vacuum oven (0.5 psia) for 12 h.[30] The PEI loading of resin-templated sorbents was determined using a TGA with continuous air purge. The heating protocol comprises a ramp at 5 °C/min from room temperature to 900 °C.

2.5. CO_2 Sorption Measurements. CO_2 sorption isotherms at 35 °C were measured using an ASAP 2020Plus physisorption analyzer (Micromeritics, Norcross, GA) at pressures up to 1 atm. Sorbent samples were degassed at 110 °C for 3 h prior to isotherm collection. Equilibrium CO_2 sorption measurements under a humidified CO_2/N_2 feed were carried out using a dynamic vapor sorption analyzer (VTI-SA+, TA Instruments) equipped with a dew point analyzer, allowing

https://doi.org/10.1021/acs.iecr.4c00479
Ind. Eng. Chem. Res. XXXX, XXX, XXX−XXX

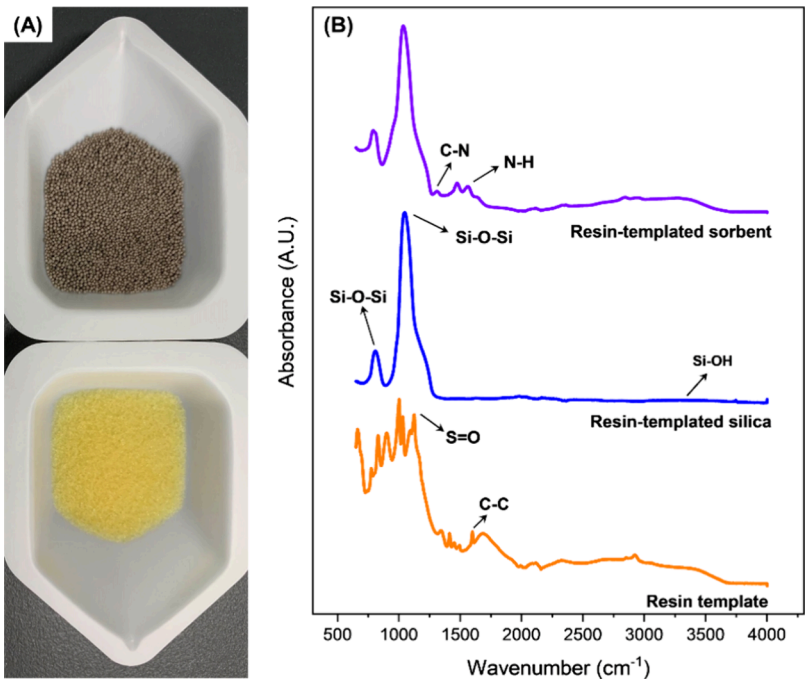

Figure 1. (A) Photographs showing the AmberLyst 15 resin template (top) and resin-templated silica (bottom). (B) FT-IR spectra of the resin template, resin-templated silica, and resin-templated sorbent impregnated with 15 wt % PEI/methanol solution.

precise control of relative humidity (RH) in the range of 5−95% (±1%). A schematic of the dynamic vapor sorption analyzer is shown in Figure S1. The analyzer was connected to a N_2 cylinder and a CO_2/N_2 cylinder by a three-way valve. The sorbent sample was loaded to the sample chamber and degassed at 110 °C for 6 h under dry N_2 purge. Once the sample was cooled to 35 °C, humidified N_2 with controlled RH was introduced to the sample chamber and sample weight gain was seen due to water sorption. Once water sorption reaches equilibrium, a humidified CO_2/N_2 feed was introduced to the sample chamber by switching the three-way valve to the CO_2/N_2 cylinder. Because the feed RH was unchanged, the CO_2 sorption capacity under humidified CO_2/N_2 feed can then be calculated based on the sample weight gain after the three-way valve was switched. An example "sample weight−time" curve of an equilibrium CO_2 sorption measurement is shown in Figure S1.

3. RESULTS AND DISCUSSION

3.1. Formation of Resin-Templated Silica. AmberLyst 15 is a hickory-colored (Figure 1A) strong acidic porous resin with a styrene-divinylbenzene matrix and sulfonic acid functional groups. In addition to being used for cation exchange, AmberLyst 15 is an acid catalyst useful for esterification,[39] hydrolysis,[40] and alkylation.[41] Vacuum-dried AmberLyst 15 resin beads were soaked in an organic silane precursor solution (10 wt % vinyltrimethoxysilane/hexane) and exposed to moist air to provide silane-treated resin templates. Air calcination of the silane-treated resin template provided resin-templated silica. The sample color change following air calcination can be noticed in Figure 1A. The percentage residual weight of the resin-templated silica was ∼6%. The large weight loss was due to decomposition of the organic ion-exchange resin template, which is evidenced by the disappearance of organic groups (S═O stretching at 1124 cm^{-1} and C═C stretching at 1598 cm^{-1}) from the Fourier transform infrared spectroscopy (FT-IR, Figure 1B) spectra of the resin-templated silica. According to EDX, the resin-templated silica is fully inorganic consisting of silicon and oxygen (Figure S2) with carbon and sulfur removed. The silica formation was further confirmed by FT-IR, which showed Si−O−Si peaks at 1090 and 800 cm^{-1}. A weak silanol peak (Si−OH) was also observed at 3400 cm^{-1}.

Although a large weight loss occurred during air calcination, scanning electron microscopy (SEM) shows that the resin-templated silica retained the structural integrity and spherical shape of the resin template with reduced diameters. While the resin template (Figure 2A) has an average diameter of 727 μm, the resin-templated silica (Figure 2C) has an average diameter of 412 μm (Figure S3). Notably, SEM suggests that the porous structure of the resin template was retained in the resin-templated silica. The resin template has an asymmetric structure, with a porous core covered by an apparently dense shell (Figure 2B). Interestingly, this asymmetric structure was reproduced in resin-templated silica (Figure 2D). Formation of resin-templated silica is believed to follow the same mechanism of petrified hollow fiber membranes reported in our previous work.[33] Indeed, both resin-templated silica and the petrified hollow fiber membrane reproduce the shape and asymmetry of their polymer templates.

3.2. Pore Structure of Resin-Templated Silica. The pore structure of the AmberLyst 15 resin template and resin-templated silica was studied by nitrogen (N_2) physisorption at 77 K (Figure 3A and Table 1). The resin template showed a Type I N_2 physisorption isotherm with a low Brunauer−Emmett−Teller (BET) surface area ∼37 m^2/g (BET plots shown in Figure S4). The resin-templated silica showed a much higher BET surface area (∼636 m^2/g) than the resin template. The hierarchical meso-/macroporous structure of the resin-templated silica was evidenced by increasing N_2 adsorption capacity at relative pressure (P/P_0) of 0.6−1.0 and the hysteresis loop. Notably, the hysteresis loop of the

https://doi.org/10.1021/acs.iecr.4c00479
Ind. Eng. Chem. Res. XXXX, XXX, XXX−XXX

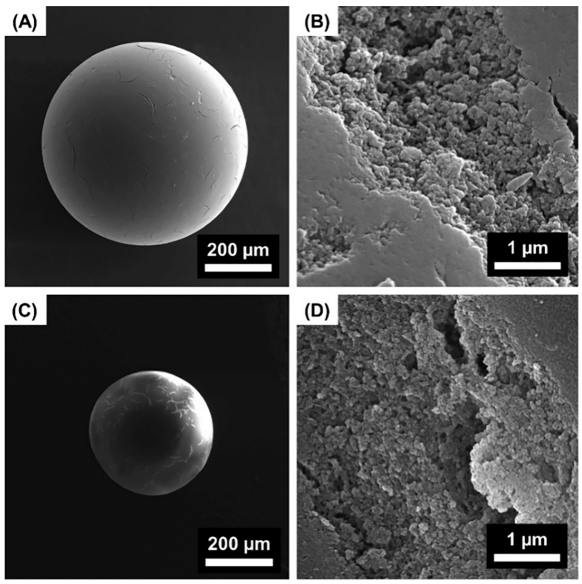

Figure 2. Scanning electron microscope images of the AmberLyst 15 resin template and resin-templated silica. (A) Overview of a resin template particle. (B) Macropores of resin template. (C) Overview of a resin-templated silica particle. (D) Macropores of resin-templated silica.

resin-templated silica is broader than those seen in ordered mesoporous silica such as MCM-41 or SBA-15,[42−44] suggesting that the resin-templated silica had less uniform mesopore size distribution. The mesopores in the resin-templated silica were further quantified by pore size distribution (Figure 3B) obtained by analyzing the N_2 physisorption isotherms using the nonlocal density functional theory (NLDFT). The pore size distribution curve indicates that the resin-templated silica has mesopores as small as 2 nm. These small mesopores are possibly responsible for the high N_2 adsorption at $P/P_0 < 0.1$. NLDFT also allowed for the calculation of cumulative surface area (Figure 3C) and cumulative pore volume (Figure 3D) of the resin-templated silica.

In addition to N_2 physisorption, mercury intrusion porosimetry (MIP, Figure S5) was performed to give pore size distribution, cumulative surface area, and cumulative pore volume for the resin template and resin-templated silica. Compared with the resin template, the resin-templated silica had larger porosity, lower bulk density, and almost identical skeletal density (Table S1). Although the AmberLyst 15 resin was labeled as macroporous by the manufacturer, mercury intrusion porosimetry shows that it is in fact dominated by mesopores of ∼20 nm. Following petrification, the resin-templated silica showed smaller mesopore size yet larger mesopore volume. This is consistent with our prior observation in petrified hollow fiber membranes.[33] It should be noted that although the resin-templated silica has both meso- and macropores, its pore volume is dominated by mesopores. Although a mismatch was seen in the pore size distribution curves of resin-templated silica obtained by NLDFT and MIP, the two methods showed quite close total surface areas and pore volume. It should be noted that the total surface area measured by NLDFT (∼480 m^2/g) and MIP (∼518 m^2/g) were both lower than the BET surface area (∼636 m^2/g). This is because NLDFT cannot measure pores larger than 40 nm and MIP cannot measure pores smaller than 3 nm, whereas the BET method can measure surface area in the full micro-/meso-/macropore size range.

Mesoporosity of the resin-templated silica was also evidenced by a hysteresis loop on the water adsorption isotherm (Figure S6A). The resin-templated silica showed comparable water uptake (∼45 wt %) with commercial silica desiccants. Analysis of the water adsorption isotherms (Figure S6B) measured at 15, 25, and 35 °C using the Clausius−Clapeyron equation allowed to calculate the water isosteric heats of adsorption (Figure S6C).[45] The higher isosteric heats of adsorption at lower water loadings represent a strong interaction between water molecules and surface silanol groups in the hydrophilic resin-templated silica. As the water loading increased, the isosteric heat of adsorption dropped and approached the water heat of vaporization. This was because the water−water interaction dominates capillary condensation in macropores and large mesopores, which occurred at higher relative humidity (higher water loading).

3.3. Effect of Calcination Temperature on the Pore Structure of Resin-Templated Silica. We further investigated the effects of the air calcination temperature (400−800 °C) on the pore structure of resin-templated silica. As the calcination temperature increased from 400 to 500 °C, both N_2 physisorption capacity (Figure 4A) and BET surface area (Figure 4B) of the resin-templated silica increased. Analysis of the N_2 physisorption isotherm by NLDFT suggested that the pore volume (Figure 4B) also increased. The increase in surface area and pore volume was possibly due to thermal decomposition of the organic resin template and formation of porous silica structure. As the calcination temperature continued to increase from 500 to 800 °C, the resin-templated silica showed reduced N_2 physisorption capacity, BET surface area, and pore volume, which was likely due to densification of the porous silica structure. The highest surface area (748 m^2/g) and pore volume (1.45 cm^3/g) were obtained at an air calcination temperature of 500 °C. The resin-templated silica made at 400−800 °C showed similarly shaped mesopore size distribution curves (Figure 4C). Compared with hierarchically meso-/macroporous silica reported in the literature (Figure 4D and Table S2), the resin-templated silica has an attractive total surface area.

3.4. Role of Resin Template Pores in Formation of Resin-Templated Silica. We studied the role of resin template pores in the formation of resin-templated silica. AmberLite FPC23H is a strong acidic macroporous cation-exchange resin with similar chemistry (styrene-divinylbenzene matrix and sulfonic acid functional groups) with the AmberLyst 15 resin. The resin-templated silica derived from the FPC23H resin template had lower BET surface area (213 m^2/g, Figure S7) than the resin-templated silica derived from the AmberLyst 15 resin template, which can be attributed to the lower BET surface area (15 m^2/g) of the FPC23H resin template. AmberLite IRC120H is a strong acidic cation-exchange resin with similar chemistry (styrene-divinylbenzene matrix and sulfonic acid functional groups) with the AmberLyst 15 resin. Unlike the AmberLyst 15 resin, however, AmberLite IRC120H is a nonporous gel-type resin. Petrification of the AmberLite IRC120H resin did not provide spherical resin-templated silica (Figure S8). Instead, irregularly shaped silica fragments were obtained with much lower residual weight (<1%) than the resin-templated silica derived from AmberLyst 15 (∼6%). Unlike the porous resin-templated silica derived from AmberLyst 15, the silica fragments derived

https://doi.org/10.1021/acs.iecr.4c00479
Ind. Eng. Chem. Res. XXXX, XXX, XXX−XXX

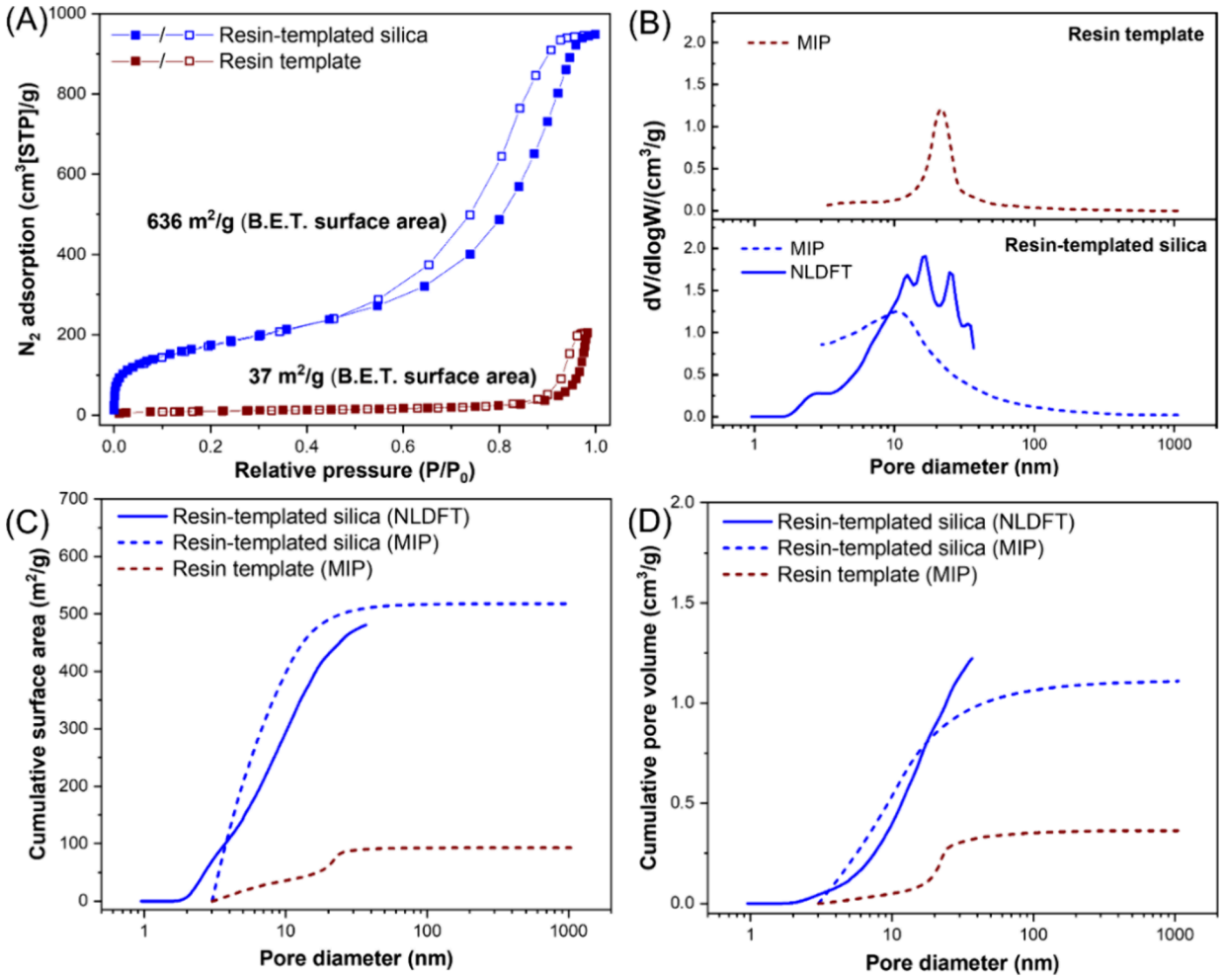

Figure 3. Pore structure of the AmberLyst 15 resin template and resin-templated silica. (A) N_2 physisorption isotherm (77K) in the resin template and resin-templated silica. The solid points represent the adsorption branch, and the hollow points represent the desorption branch; (B) pore size distribution curves of the resin template (obtained from MIP) and resin-templated silica (obtained from MIP and NLDFT); (C) cumulative surface area of the resin template (obtained from MIP) and resin-templated silica (obtained from MIP and NLDFT); (D) cumulative pore volume of the resin template (obtained from MIP) and resin-templated silica (obtained from MIP and NLDFT).

Table 1. Comparing Surface Area and Pore Volume of the AmberLyst 15 Resin Template and Resin-Templated Silica[a]

	surface area (m^2/g)			pore volume (cm^3/g)	
material	BET	NLDFT	MIP	NLDFT	MIP
resin template	37	N/A	93	N/A	0.36
resin-templated silica	636	480	518	1.22	1.10

[a]Surface areas were determined by BET, NLDFT, and MIP methods. Pore volumes were determined by the NLDFT and MIP methods.

from AmberLite IRC120H was nonporous with low BET surface area (~39 m^2/g). Based on these results, we postulate that pores in the resin template are crucial to the formation of resin-templated silica with hierarchical meso-/macropores and high surface area. The pores in resin templates possibly provided space for silane precursor impregnation and the subsequent silica formation during petrification.[33]

The role of resin template pores in the formation of resin-templated silica underscores the differences between the dual-templated silica prepared by Kwon and co-workers[30] and the resin-templated silica reported in this work. While preformed spherical polymer templates are used for both, dual-templated silica relies on small (diameter ~1 μm) and nonporous template (polystyrene beads) and resin-templated silica relies on much larger (diameter ~727 μm) and macroporous template (ion-exchange resin beads). Both dual-templated silica and resin-templated silica have hierarchical meso-/macropores yet different pore size uniformity. Dual-templated silica has uniform mesopores and macropores, which are formed by removal of assembled surfactant templates and removal of preformed polystyrene templates, respectively. Resin-templated silica has nonuniform macropores and mesopores and are both formed by removal of preformed ion-exchange resin templates. At the same calcination temperature of 550 °C, the resin-templated silica shows a larger surface area (626 vs 448 m^2/g) and smaller pore volume (1.27 vs 4.52 cm^3/g) than the dual-templated silica.

3.5. CO_2 Capture by PEI-Impregnated Resin-Templated Sorbents. The hierarchical meso-/macroporosity of the resin-templated silica makes them attractive substrates to fabricate amine-impregnated CO_2 capture sorbents, that is, resin-templated sorbents. The amine impregnation was carried out by soaking the resin-templated silica substrates in 5, 15, and 25 wt % polyethylenimine (PEI, M_w ~ 800, branched)/methanol solution followed by vacuum drying. Successful

https://doi.org/10.1021/acs.iecr.4c00479
Ind. Eng. Chem. Res. XXXX, XXX, XXX−XXX

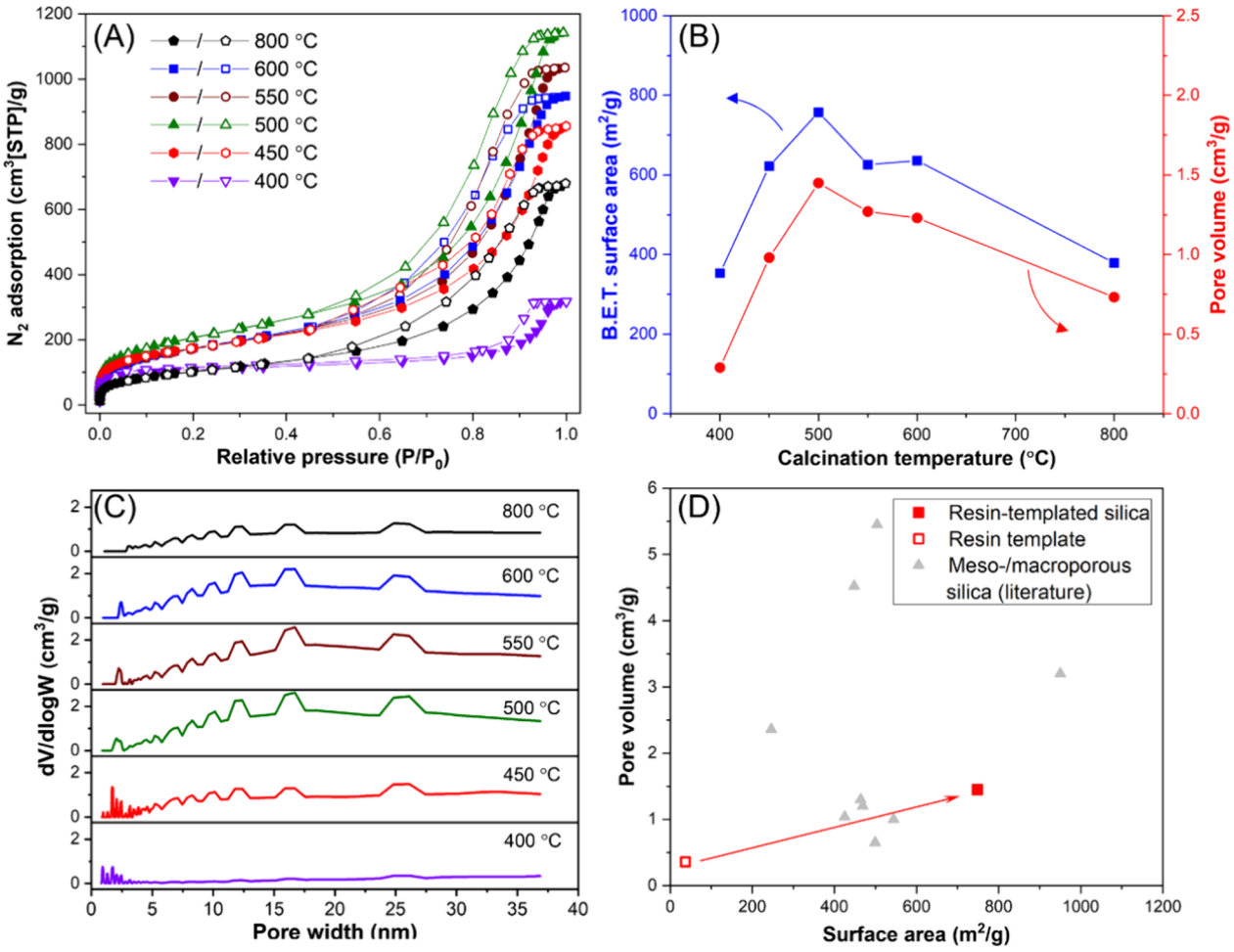

Figure 4. Effect of air calcination temperature on the pore structure of resin-templated silica derived from the AmberLyst 15 resin template. (A) N_2 physisorption isotherms (77K). The solid points represent the adsorption branch, and the hollow points represent the desorption branch; (B) BET surface area and pore volume (obtained from NLDFT); (C) pore size distribution curves of resin-templated silica (obtained from NLDFT); (D) comparing the surface area and pore volume of resin-templated silica with meso-/macroporous silica reported in the literature. The surface area of resin-templated silica was determined by the BET method. The pore volume of resin-templated silica was determined by NLDFT.

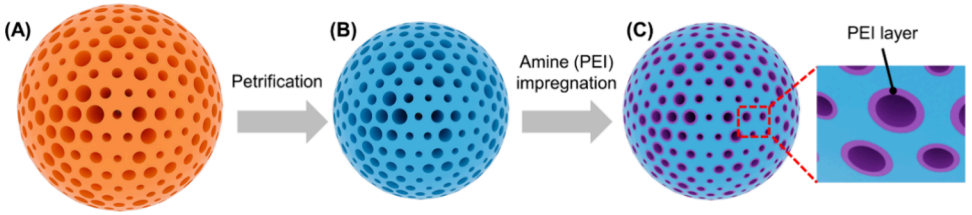

Figure 5. Schematics illustrating formation of resin-templated sorbents. (A) Resin template. (B) Resin-templated silica substrate. (C) Resin-templated sorbents formed by impregnation of the resin-templated silica substrate with polyethylenimine (PEI).

impregnation was evidenced by the appearance of C−N and N−H peaks in the FT-IR spectra (Figure 1B). The sorbent amine loading was determined by TGA (Figure S9A), which showed that the resin-templated sorbents impregnated with 5, 15, and 25 wt % PEI/methanol solutions had amine loading of 0.25, 0.83, and 1.35 g PEI/g SiO_2, respectively (Table S3). Figure 5 shows a schematic of amine impregnation in resin-templated silica substrates. The resin-templated sorbent showed a similar morphology to the resin-templated silica. Following PEI impregnation, the resin-templated sorbent particles (Figure S9B) remained spherical with macropores (Figure S9C) seen on the outer surface. The resin-templated sorbent showed much lower N_2 physisorption (77 K) capacity (Figure S9D) with smaller mesopore volume (Figure S9E). This was due to partially filling the mesopore space with PEI. The reduction in mesopore volume after PEI impregnation was consistent with the observation by Kwon and co-workers.[30]

The CO_2 sorption isotherms (Figure 6) of the resin-templated silica and resin-templated sorbents were measured at 35 °C and pressures up to 1 bar. The resin-templated silica had a low CO_2 sorption capacity, likely due to the lack of chemisorption sites. The impregnated PEI in the resin-templated sorbent provided dramatically higher CO_2 sorption capacity, which increased with amine loading. The highest amine efficiency (Table S3) was obtained in the resin-templated sorbent made with 15 wt % PEI/methanol solution

https://doi.org/10.1021/acs.iecr.4c00479
Ind. Eng. Chem. Res. XXXX, XXX, XXX−XXX

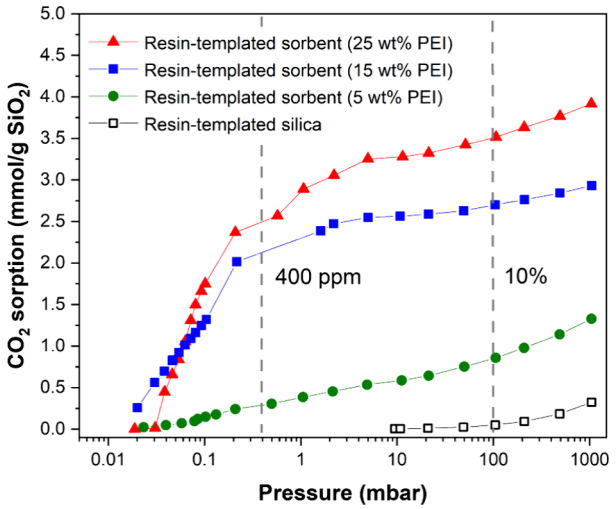

Figure 6. CO_2 sorption isotherms (35 °C) in resin-templated silica substrate and resin-templated sorbents impregnated with 5, 15, and 25 wt % PEI/methanol solutions. The dashed lines represent the CO_2 concentration in air (400 ppm) and flue gas (10%).

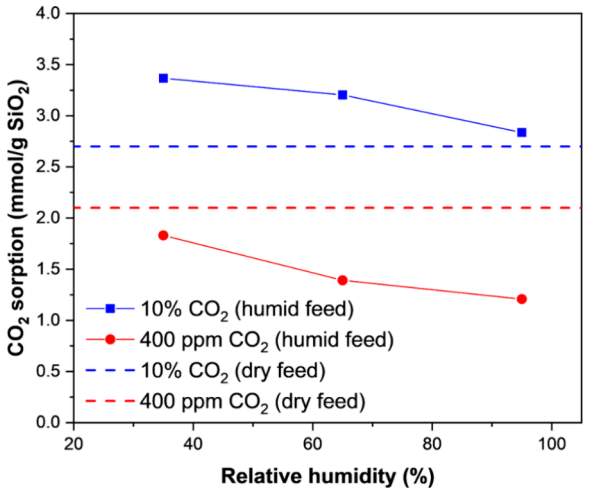

Figure 7. Effects of feed relative humidity on CO_2 sorption capacity (35 °C) in resin-templated sorbent impregnated with 15 wt % PEI/methanol solution. The dashed lines represent the CO_2 sorption capacity under dry feed conditions.

showing a CO_2 sorption capacity of 2.1 mmol/g SiO_2 for direct air capture (at 0.004 bar) and 2.7 mmol/g SiO_2 for flue gas capture (at 0.1 bar). The lower amine efficiency in the resin-templated sorbent impregnated with 25 wt % PEI/methanol solution was possibly due to thicker amine films and slower CO_2 sorption kinetics.[4] As reported by Kwon and co-workers,[30] the effects of amine film thickness on CO_2 sorption kinetics is more pronounced at low CO_2 concentration, which is responsible for the lower CO_2 sorption capacity in the resin-templated sorbent impregnated with 25 wt % PEI/methanol solution at CO_2 pressure below 0.06 mbar. At comparable amine loading and feed conditions, the resin-templated sorbent showed competitive CO_2 sorption capacity for direct air capture with a hierarchical meso-/macroporous silica sorbent reported in the literature.[30]

Using a dynamic vapor sorption analyzer, we studied the effects of feed relative humidity (RH) on the CO_2 sorption capacity of the resin-templated sorbent impregnated with 15 wt % PEI/methanol solution (Figure 7). In general, the presence of feedwater vapor enhances the uptake capacity of amine-oxide sorbents by facilitating the formation of carbonate and bicarbonate species.[4] For the feed with 10% CO_2, feedwater vapor enhanced the CO_2 sorption capacity over the CO_2 sorption capacity measured under dry feed (Figure 6). The CO_2 sorption capacity was reduced as the feed RH increased from 35 to 95% (Figure 7). This was possibly due to unfavorable CO_2 sorption kinetics as the amines were oversaturated with water at higher RH. Another possibility is deactivation of amine sites due to urea formation.[46] The CO_2 sorption capacity was lower at 400 ppm of CO_2 under each feed RH. Kwon and co-workers[30] reported that CO_2 sorption is more kinetically limited at 400 ppm of CO_2 than at 10% CO_2, thereby giving lower sorption capacity at 400 ppm. This was likely responsible for the lower CO_2 sorption capacity at 400 ppm of CO_2 under each feed RH.

4. CONCLUSIONS

To summarize, we reported fabrication of resin-templated silica, a novel class of hierarchically meso-/macroporous materials made by petrification of porous ion-exchange resin templates via three simple steps of silane soaking, moisture exposure, and air calcination. The resin-templated silica had a good surface area (748 m^2/g) and pore volume (1.45 cm^3/g), which were both much higher than those of the porous ion-exchange resin template. Compared with ordered mesoporous silica, resin-templated silica had a broader pore size distribution. It was found that nonporous gel-type resins cannot provide resin-templated silica due to lack of pores. Impregnation of the resin-templated silica using 15 wt % PEI/methanol solution provided resin-templated sorbents with attractive CO_2 sorption capacity for direct air capture (2.1 mmol of CO_2/g of SiO_2) at an amine loading of 0.83 g of PEI/g of SiO_2 and an amine efficiency of 0.11 mol of CO_2/mol of N. To our best knowledge, this was the first time that mesoporous silica was derived from ion-exchange resin templates. Compared with traditional amine-oxide sorbents relying on ordered mesoporous silica substrates, the novel resin-templated sorbents reported in this work are potentially competitive due to the streamlined silica substrate fabrication without using surfactants or block copolymer templates.

■ ASSOCIATED CONTENT

Supporting Information

The Supporting Information is available free of charge at https://pubs.acs.org/doi/10.1021/acs.iecr.4c00479.

Energy dispersive X-ray analysis results, particle size distribution curves, BET plots, mercury intrusion data, results of silica derived from gel-type AmberLite IRC120H resin, water vapor adsorption isotherms, and TGA plots of the resin-templated sorbents (PDF)

■ AUTHOR INFORMATION

Corresponding Author

Chen Zhang − *Department of Chemical and Biomolecular Engineering, University of Maryland, College Park, Maryland 20742, United States;* orcid.org/0000-0002-0071-2898; Email: czhang71@umd.edu

https://doi.org/10.1021/acs.iecr.4c00479
Ind. Eng. Chem. Res. XXXX, XXX, XXX−XXX

Authors

Ching-En Ku − *Department of Chemical and Biomolecular Engineering, University of Maryland, College Park, Maryland 20742, United States*

Lu Liu − *Department of Chemical and Biomolecular Engineering, University of Maryland, College Park, Maryland 20742, United States*

Complete contact information is available at: https://pubs.acs.org/10.1021/acs.iecr.4c00479

Author Contributions

The manuscript was written through contributions of all authors. All authors have given approval to the final version of the manuscript.

Funding

This work was supported by the National Science Foundation under Award CBET-2044794.

Notes

The authors declare no competing financial interest.

■ ACKNOWLEDGMENTS

C.Z. thanks faculty summer support from the Minta Martin Award. C.-E.K. thanks the Wells Fellowship provided by the Maryland Energy Innovation Institute. L.L. is grateful for the Hulka Energy Research Fellowship provided by the Maryland Energy Innovation Institute. The authors thank D. Liu and the A. J. Clark Hall Materials Characterization Lab for kindly providing access to TGA instrument. The authors also acknowledge the support of the Maryland NanoCenter and its AIMLab.

■ REFERENCES

(1) Sanz-Perez, E. S.; Murdock, C. R.; Didas, S. A.; Jones, C. W. Direct Capture of CO_2 from Ambient Air. *Chem. Rev.* **2016**, *116* (19), 11840−11876.

(2) National Academies of Sciences, E.; Medicine, *Negative Emissions Technologies and Reliable Sequestration: A Research Agenda*. The National Academies Press: Washington, DC, 2019; p 510.

(3) Voskian, S.; Hatton, T. A. Faradaic electro-swing reactive adsorption for CO_2 capture. *Energy Environ. Sci.* **2019**, *12* (12), 3530−3547.

(4) Bollini, P.; Didas, S. A.; Jones, C. W. Amine-oxide hybrid materials for acid gas separations. *J. Mater. Chem.* **2011**, *21* (39), 15100−15120.

(5) Didas, S. A.; Choi, S.; Chaikittisilp, W.; Jones, C. W. Amine−Oxide Hybrid Materials for CO_2 Capture from Ambient Air. *Acc. Chem. Res.* **2015**, *48* (10), 2680−2687.

(6) Szczęśniak, B.; Choma, J.; Jaroniec, M. Major advances in the development of ordered mesoporous materials. *Chem. Commun.* **2020**, *56* (57), 7836−7848.

(7) Kresge, C. T.; Leonowicz, M. E.; Roth, W. J.; Vartuli, J. C.; Beck, J. S. Ordered mesoporous molecular sieves synthesized by a liquid-crystal template mechanism. *Nature* **1992**, *359* (6397), 710−712.

(8) Xu, X.; Song, C.; Andresen, J. M.; Miller, B. G.; Scaroni, A. W. Novel Polyethylenimine-Modified Mesoporous Molecular Sieve of MCM-41 Type as High-Capacity Adsorbent for CO_2 Capture. *Energy Fuels* **2002**, *16* (6), 1463−1469.

(9) Min, Y. J.; Ganesan, A.; Realff, M. J.; Jones, C. W. Direct Air Capture of CO_2 Using Poly(ethyleneimine)-Functionalized Expanded Poly(tetrafluoroethylene)/Silica Composite Structured Sorbents. *ACS Appl. Mater. Interfaces* **2022**, *14* (36), 40992−41002.

(10) Moon, H. J.; Carrillo, J.-M.; Leisen, J.; Sumpter, B. G.; Osti, N. C.; Tyagi, M.; Jones, C. W. Understanding the Impacts of Support−Polymer Interactions on the Dynamics of Poly(ethyleneimine) Confined in Mesoporous SBA-15. *J. Am. Chem. Soc.* **2022**, *144* (26), 11664−11675.

(11) Sujan, A. R.; Kumar, D. R.; Sakwa-Novak, M.; Ping, E. W.; Hu, B.; Park, S. J.; Jones, C. W. Poly(glycidyl amine)-Loaded SBA-15 Sorbents for CO_2 Capture from Dilute and Ultradilute Gas Mixtures. *ACS Appl. Polym. Mater.* **2019**, *1* (11), 3137−3147.

(12) Li, K.; Jiang, J.; Yan, F.; Tian, S.; Chen, X. The influence of polyethyleneimine type and molecular weight on the CO_2 capture performance of PEI-nano silica adsorbents. *Appl. Energy* **2014**, *136*, 750−755.

(13) Kumar, P.; Guliants, V. V. Periodic mesoporous organic−inorganic hybrid materials: Applications in membrane separations and adsorption. *Microporous Mesoporous Mater.* **2010**, *132* (1), 1−14.

(14) Chaikittisilp, W.; Didas, S. A.; Kim, H.-J.; Jones, C. W. Vapor-Phase Transport as A Novel Route to Hyperbranched Polyamine-Oxide Hybrid Materials. *Chem. Mater.* **2013**, *25* (4), 613−622.

(15) Choi, S.; Drese, J. H.; Jones, C. W. Adsorbent Materials for Carbon Dioxide Capture from Large Anthropogenic Point Sources. *ChemSusChem* **2009**, *2* (9), 796−854.

(16) Labreche, Y.; Fan, Y.; Lively, R. P.; Jones, C. W.; Koros, W. J. Direct dual layer spinning of aminosilica/Torlon® hollow fiber sorbents with a lumen layer for CO_2 separation by rapid temperature swing adsorption. *J. Appl. Polym. Sci.* **2015**, *132* (17), 41845.

(17) Fan, Y.; Kalyanaraman, J.; Labreche, Y.; Rezaei, F.; Lively, R. P.; Realff, M. J.; Koros, W. J.; Jones, C. W.; Kawajiri, Y. CO_2 Sorption Performance of Composite Polymer/Aminosilica Hollow Fiber Sorbents: An Experimental and Modeling Study. *Ind. Eng. Chem. Res.* **2015**, *54* (6), 1783−1795.

(18) Fan, Y.; Lively, R. P.; Labreche, Y.; Rezaei, F.; Koros, W. J.; Jones, C. W. Evaluation of CO_2 adsorption dynamics of polymer/silica supported poly(ethylenimine) hollow fiber sorbents in rapid temperature swing adsorption. *Int. J. Greenhouse Gas Control* **2014**, *21*, 61−71.

(19) Li, F. S.; Lively, R. P.; Lee, J. S.; Koros, W. J. Aminosilane-Functionalized Hollow Fiber Sorbents for Post-Combustion CO_2 Capture. *Ind. Eng. Chem. Res.* **2013**, *52* (26), 8928−8935.

(20) Guo, X.; Ding, L.; Kanamori, K.; Nakanishi, K.; Yang, H. Functionalization of hierarchically porous silica monoliths with polyethyleneimine (PEI) for CO_2 adsorption. *Microporous Mesoporous Mater.* **2017**, *245*, 51−57.

(21) Petkovich, N. D.; Stein, A. Controlling macro- and mesostructures with hierarchical porosity through combined hard and soft templating. *Chem. Soc. Rev.* **2013**, *42* (9), 3721−3739.

(22) Zhao, D.; Feng, J.; Huo, Q.; Melosh, N.; Fredrickson, G. H.; Chmelka, B. F.; Stucky, G. D. Triblock Copolymer Syntheses of Mesoporous Silica with Periodic 50 to 300 Angstrom Pores. *Science* **1998**, *279* (5350), 548−552.

(23) Beck, J. S.; Vartuli, J. C.; Roth, W. J.; Leonowicz, M. E.; Kresge, C. T.; Schmitt, K. D.; Chu, C. T. W.; Olson, D. H.; Sheppard, E. W.; McCullen, S. B.; Higgins, J. B.; Schlenker, J. L. A new family of mesoporous molecular sieves prepared with liquid crystal templates. *J. Am. Chem. Soc.* **1992**, *114* (27), 10834−10843.

(24) Kruk, M.; Jaroniec, M.; Ko, C. H.; Ryoo, R. Characterization of the Porous Structure of SBA-15. *Chem. Mater.* **2000**, *12* (7), 1961−1968.

(25) van Grieken, R.; Calleja, G.; Stucky, G. D.; Melero, J. A.; García, R. A.; Iglesias, J. Supercritical Fluid Extraction of a Nonionic Surfactant Template from SBA-15 Materials and Consequences on the Porous Structure. *Langmuir* **2003**, *19* (9), 3966−3973.

(26) Chen, C.; Yang, S.-T.; Ahn, W.-S.; Ryoo, R. Amine-impregnated silica monolith with a hierarchical pore structure: enhancement of CO_2 capture capacity. *Chem. Commun.* **2009**, *24*, 3627−3629.

(27) Han, Y.; Hwang, G.; Kim, H.; Haznedaroglu, B. Z.; Lee, B. Amine-impregnated millimeter-sized spherical silica foams with hierarchical mesoporous−macroporous structure for CO_2 capture. *Chem. Eng. J.* **2015**, *259*, 653−662.

(28) Witoon, T.; Chareonpanich, M. Synthesis of hierarchical meso-macroporous silica monolith using chitosan as biotemplate and its

application as polyethyleneimine support for CO_2 capture. *Mater. Lett.* **2012**, *81*, 181−184.
(29) Qi, G.; Fu, L.; Choi, B. H.; Giannelis, E. P. Efficient CO_2 sorbents based on silica foam with ultra-large mesopores. *Energy Environ. Sci.* **2012**, *5* (6), 7368−7375.
(30) Kwon, H. T.; Sakwa-Novak, M. A.; Pang, S. H.; Sujan, A. R.; Ping, E. W.; Jones, C. W. Aminopolymer-Impregnated Hierarchical Silica Structures: Unexpected Equivalent CO_2 Uptake under Simulated Air Capture and Flue Gas Capture Conditions. *Chem. Mater.* **2019**, *31* (14), 5229−5237.
(31) Forster, T.; Scholz, S.; Zhu, Y. Z.; Lercher, J. A. One step synthesis of organofunctionalized transition metal containing meso- and macroporous silica spheres. *Microporous Mesoporous Mater.* **2011**, *142* (2−3), 464−472.
(32) Feinle, A.; Akbarzadeh, J.; Peterlik, H.; Husing, N. Ordered meso-/macroporous silica and titania films by breath figure templating in combination with non-hydrolytic sol-gel processing. *Microporous Mesoporous Mater.* **2015**, *217*, 233−243.
(33) Liu, L.; Ku, C.-E.; Zhang, C. Petrified Hollow Fiber Membranes with Hierarchical Pores. *ACS Mater. Lett.* **2022**, *4* (5), 938−943.
(34) Lee, J. C.; Kurniawan; Hong, H. J.; Chung, K. W.; Kim, S. Separation of platinum, palladium and rhodium from aqueous solutions using ion exchange resin: A review. *Sep. Purif. Technol.* **2020**, *246*, No. 116896.
(35) Bratek, K.; Bratek, W.; Kulazynski, M. Carbon adsorbents from waste ion-exchange resin. *Carbon* **2002**, *40* (12), 2213−2220.
(36) Madureira, A.; Noel, S.; Leger, B.; Ponchel, A.; Monflier, E. Catalytic Hydrogenation of Derived Vegetable Oils Using Ion-Exchange Resin-Supported Ruthenium Nanoparticles: Scope and Limitations. *ACS Sustainable Chem. Eng.* **2022**, *10*, 16588.
(37) Wagh, K. V.; Bhanage, B. M. Amberlyst-15/ Bmim PF6 Catalyzed Synthesis of C-3-Symmetric Triarylbenzenes via Cyclotrimerization of Alkynes. *ACS Sustainable Chem. Eng.* **2016**, *4* (8), 4232−4236.
(38) Sakurai, H.; Koga, K.; Kiuchi, M. Gold nanoparticles deposited on Amberlyst-15: Metal-acid bifunctional catalyst for cellobiose conversion to gluconic acid. *Catal. Today* **2015**, *251*, 96−102.
(39) Melfi, D. T.; Lenzi, M. K.; Ramos, L. P.; Corazza, M. L. Kinetic Modeling of $scCO_2$-Assisted Levulinic Acid Esterification with Ethanol Using Amberlyst-15 as a Catalyst in a Batch Reactor. *Energy Fuels* **2021**, *35* (18), 14770−14779.
(40) Nguyen, V. C.; Bui, N. Q.; Mascunan, P.; Vu, T. T. H.; Fongarland, P.; Essayem, N. Esterification of aqueous lactic acid solutions with ethanol using carbon solid acid catalysts: Amberlyst 15, sulfonated pyrolyzed wood and graphene oxide. *Appl. Catal., A* **2018**, *552*, 184−191.
(41) Qureshi, Z. S.; Deshmukh, K. M.; Tambade, P. J.; Dhake, K. P.; Bhanage, B. M. Amberlyst-15 in Ionic Liquid: An Efficient and Recyclable Reagent for Nucleophilic Substitution of Alcohols and Hydroamination of Alkenes. *EurJOC* **2010**, *2010* (32), 6233−6238.
(42) Thommes, M.; Schlumberger, C. Characterization of Nanoporous Materials. *Annu. Rev. Chem. Biomol. Eng.* **2021**, *12* (1), 137−162.
(43) Zukal, A.; Thommes, M.; Čejka, J. Synthesis of highly ordered MCM-41 silica with spherical particles. *Microporous Mesoporous Mater.* **2007**, *104* (1), 52−58.
(44) Thommes, M. Physical Adsorption Characterization of Nanoporous Materials. *Chem. Ing. Technol.* **2010**, *82* (7), 1059−1073.
(45) Zhang, K.; Lively, R. P.; Zhang, C.; Koros, W. J.; Chance, R. R. Investigating the Intrinsic Ethanol/Water Separation Capability of ZIF-8: An Adsorption and Diffusion Study. *J. Phys. Chem. C* **2013**, *117* (14), 7214−7225.
(46) Sayari, A.; Belmabkhout, Y. Stabilization of Amine-Containing CO_2 Adsorbents: Dramatic Effect of Water Vapor. *J. Am. Chem. Soc.* **2010**, *132* (18), 6312−6314.

https://doi.org/10.1021/acs.iecr.4c00479
Ind. Eng. Chem. Res. XXXX, XXX, XXX−XXX